JOURNAL OF THERMOPHYSICS AND HEAT TRANSFER
Vol. 6, No. 2, April–June 1992

Effects of g-Jitter on a Thermally Buoyant Flow

F. Tsau,* S. Elghobashi,† and W. A. Sirignano‡
University of California at Irvine, Irvine, California 92717

The effects of g-jitter on a three-dimensional, thermally buoyant laminar flow in a cylindrical enclosure is examined via a finite difference method. The enclosure is heated nonuniformly from above and a periodic gravitational acceleration is imposed on the flow to simulate gravity jittering. The study finds that the flowfield, responding to the imposed gravitational acceleration, exhibits periodic behavior and that the heat transfer rate to the fluid is increased compared to the case without g-jitter. The results also indicate that all components of the gravitational acceleration contribute to the increase of heat transfer rate but in ways different in nature. The flow at times does not remain in phase with the imposed gravity field and hot, isolated packets of fluid are found away from the heat source. A reduction of the magnitude of gravity is more efficient than just restoring the preperturbed gravity field in eliminating the effects of g-jitter after a system has been disturbed. Postjittering behavior of the flow depends on the g-jitter history and the kinematic viscosity of the working fluid.

Nomenclature

A = R/L
c_p = specific heat at constant pressure, c_p'/c_{p0}'
E = Euler constant, $p_0'/(\rho_0' u_0'^2)$
Gr = Grashof number, $g'\beta(T_w' - T_0')L^3/\nu_0'^2$
g' = gravitational acceleration, cm/s^2
L = height of the enclosure, cm
P = period of the g-jitter motion, s
Pr = Prandtl number, ν_0'/α_0'
p = pressure, $(p' - p_s')/p_0'$
R = radius of the enclosure, cm
Re = Reynolds number, $u_0'L/\nu_0'$
r = radial coordinate, r'/R
T = temperature, $(T' - T_0')/(T_w' - T_0')$
t = nondimensional time, $u_0't'/L$
u = radial velocity, u'/u_0'
V = nondimensional computational cell volume
v = circumferential velocity, v'/u_0'
w = axial velocity, w'/u_0'
z = axial coordinate, z'/L
α_0' = thermal diffusivity, cm^2/s
β = thermal expansion coefficient, K^{-1}
θ = circumferential coordinate
κ = thermal conductivity, κ'/κ_0'
μ = viscosity, μ'/μ_0'
ν = kinematic viscosity, ν'/ν_0'
ρ = density, ρ'/ρ_0'
Ω = angle between the gravity vector and positive z direction

Subscripts
r = radial component
s = hydrostatic condition
w = condition at the heat source
z = axial component
θ = circumferential component
0 = reference or initial condition

Superscript
$'$ = dimensional quantity

Introduction

THE research facilities aboard the Space Shuttle and future space station provide excellent opportunities to study the effects of external acceleration on heat and mass transfer of an engineering system under microgravity conditions. These opportunities usher in a new era in which the fundamental understanding of important transport phenomena can be enhanced. In particular, research on the behavior of fluids responding to the change (in both magnitude and orientation) of gravity has several merits. In materials engineering, the process of crystallization is known to be crucial for the properties of the final products and very sensitive to gravitational conditions. In combustion science, the buoyancy force becomes important in many situations. For instance, it is one of the responsible mechanisms[1] of heat transfer in the early stages of a flame propagating over a liquid-fuel pool, but its effects are difficult to isolate under experimentation only at Earth's gravity condition. There are various sources of external acceleration other than gravity aboard a space vehicle, e.g., sudden accelerations of the vehicle and crew movement. These external accelerations constitute modulations to the local gravity field in a space environment. It is expected that the conclusions derived from this study are applicable to situations when the history of the acceleration is similar.

Aziz and Hellums[2] were the first to solve a three-dimensional natural convection problem in an enclosure. A vorticity-vector-potential approach was devised to attack the problem, and only low Grashof number flows were examined. Ozoe et al.[3] presented the first numerical results of fluid motion and heat transfer in the multicellular regime within an inclined rectangular enclosure whose length-to-height ratio is 7. Their calculations were confined in one cell with the enclosure's length-to-height ratio and for a Prandtl number and a Rayleigh number of 10 and 4000, respectively. The enclosure was heated from below and inclined about an axis parallel to the longest dimension (width). Their single-roll cell model assumed complete similarity among roll cells with the axis of circulation parallel to the width of the enclosure so that numerical simulations could be conducted for only one cell, with proper boundary conditions assigned to the cell boundaries. A steady-state solution was sought for the velocity and temperature fields with respect to the inclination angle, and it

Presented as Paper 90-0653 at the AIAA 28th Aerospace Sciences Meeting, Reno, NV, Jan. 8–11, 1990; received Aug. 17, 1990; revision received received May 28, 1991; accepted for publication June 12, 1991. Copyright © 1991 by F. Tsau, S. Elghobashi, and W. A. Sirignano. Published by the American Institute of Aeronautics and Astronautics, Inc., with permission.

*Assistant Specialist, Department of Mechanical/Aerospace Engineering. Member AIAA.
†Professor, Department of Mechanical/Aerospace Engineering. Member AIAA.
‡Professor, Department of Mechanical/Aerospace Engineering. Fellow AIAA.

was shown that the average Nusselt number decreased to a minimum when flow transition from a multiple-cell structure to a single-cell structure occurred. Yang et al.[4] studied the three-dimensional flow transition in a tilted rectangular enclosure heated from above with numerical simulations. They validated the single-roll cell model proposed by Ozoe et al.[3] except near the end regions of the longest dimension where the single-roll cell model overpredicted the average Nusselt number. The three dimensionality in Yang's study, however, was mainly caused by wall effects, not by gravity modulations in all spatial directions. This explains the agreement and disagreement between the two studies.

Aggarwal et al.[5] examined several two-dimensional, natural convection flows in a cylindrical enclosure that was heated nonuniformly from above. They studied both the single-phase and the two-phase cases. They predicted multicellular flow structures in the single-phase case for Grashof number greater than 1.0×10^5, but this limit would increase if the adiabatic wall condition was replaced by an isothermal one. In the two-phase case, there was only one cell in the liquid phase, while both unicellular and multicellular structures were predicted in the gas phase, depending on the Grashof number. They also found that the surface tension became important when the gravity was reduced to a very low level. A related study, including effects of radiation, by Ross et al.[6] for the same geometry validated the existence of multicellular flow structure experimentally and numerically. They noted also that the temperature distribution on the heat source itself greatly influenced the flow patterns in the enclosure. Gresho and Sani[7] modulated the gravity in a sinusoidal manner and performed a linearized stability analysis on several two-dimensional flows. The modulation significantly affected the stability limits of a heated fluid layer. In particular, a heated-from-below layer can be stabilized and a heated-from-above situation can be destabilized by applying different gravity modulations. Kamotani et al.[8] in a two-dimensional study of the g-jitter effect concluded that the jittering component normal to the imposed temperature gradient was most important in generating thermal convection. They suggested further that the parallel component was probably important only in causing thermal instability, albeit no conclusive evidence was given.

Experiments that need to be conducted in space are intrinsically acceleration-sensitive, but sources of external acceleration like those mentioned above are constantly present. Moreover, those situations invariably lead to three-dimensional phenomena that make conventional two-dimensional analyses inadequate. Here, the three-dimensional effects of g-jitter are examined by using a numerical, finite difference method for an enclosure flow. The variation of the gravity occurs in all three spatial directions according to a prescribed, time-dependent function while the total magnitude remains time invariant. The numerical method employed and other numerical details are briefly described in the third section. The effects of gravity modulations on the velocity and thermal fields are presented in the fourth section by comparing the three-dimensional results with the two-dimensional results (without g-jitter) for the same geometry. The variable-property effects, the effects of each gravitational component and the postjittering behavior of the flow are also examined.

Mathematical Formulation

The flow geometry is depicted in Fig. 1 where a mass of air contained in a cylindrical enclosure is heated nonuniformly from above. The aspect ratio A of the cylinder equals unity. The gravity vector is initially aligned with the z axis and pointing in the negative z direciton. The fluid is initially quiescent at $T'_0 = 300$ K. The gravity vector then undertakes a periodic, pendulum-type motion parallel to the $\theta = 0$ (or $\theta = \pi$) plane with a maximum amplitude of $\pi/3$ relative to the negative z direction. The periods of oscillation among the cases studied are 1, 3, and 9 s, respectively. These periods cover a range below and above the characteristic time of flow recirculation

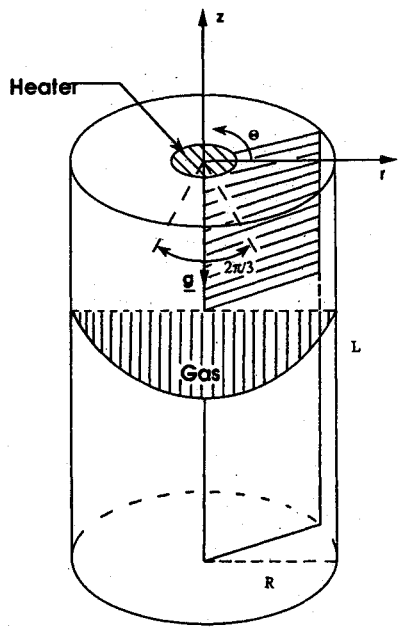

Fig. 1 Geometry, coordinate system, and cross sections displayed in the Results and Discussion section.

established without g-jitter. The unsteady, three-dimensional conservation equations of mass, momentum and energy for this flow, after being normalized by various reference quantities, are

$$A\frac{\partial \rho}{\partial t} + \frac{1}{r}\frac{\partial}{\partial r}(\rho r u) + \frac{1}{r}\frac{\partial}{\partial \theta}(\rho v) + A\frac{\partial}{\partial z}(\rho w) = 0 \quad (1)$$

$$\frac{\partial}{\partial t}(\rho u) + \frac{1}{r}\frac{\partial}{\partial r}\left[\frac{\rho r u^2}{A} - \frac{\mu r}{A^2 Re}\frac{\partial u}{\partial r}\right] + \frac{1}{r}\frac{\partial}{\partial \theta}\cdot\left[\frac{\rho v u}{A} - \frac{\mu}{rA^2 Re}\frac{\partial u}{\partial \theta}\right] + \frac{\partial}{\partial z}\left[\rho w u - \frac{\mu}{Re}\frac{\partial u}{\partial z}\right] = -\frac{E}{A}\frac{\partial p}{\partial r} + S_r + \frac{Gr}{Re^2}\frac{1-\rho}{\beta(T'_w - T'_0)}\cos(\theta)\sin(\Omega) \quad (2)$$

$$\frac{\partial}{\partial t}(\rho v) + \frac{1}{r}\frac{\partial}{\partial r}\left[\frac{\rho r u v}{A} - \frac{\mu r}{A^2 Re}\frac{\partial v}{\partial r}\right] + \frac{1}{r}\frac{\partial}{\partial \theta}\cdot\left[\frac{\rho v^2}{A} - \frac{\mu}{rA^2 Re}\frac{\partial v}{\partial \theta}\right] + \frac{\partial}{\partial z}\left[\rho w v - \frac{\mu}{Re}\frac{\partial v}{\partial z}\right] = -\frac{E}{Ar}\frac{\partial p}{\partial \theta} + S_\theta + \frac{Gr}{Re^2}\frac{\rho - 1}{\beta(T'_w - T'_0)}\sin(\theta)\sin(\Omega) \quad (3)$$

$$\frac{\partial}{\partial t}(\rho w) + \frac{1}{r}\frac{\partial}{\partial r}\left[\frac{\rho r u w}{A} - \frac{\mu r}{A^2 Re}\frac{\partial w}{\partial r}\right] + \frac{1}{r}\frac{\partial}{\partial \theta}\cdot\left[\frac{\rho v w}{A} - \frac{\mu}{rA^2 Re}\frac{\partial w}{\partial \theta}\right] + \frac{\partial}{\partial z}\left[\rho w^2 - \frac{\mu}{Re}\frac{\partial w}{\partial z}\right] = -E\frac{\partial p}{\partial z} + S_z + \frac{Gr}{Re^2}\frac{1-\rho}{\beta(T'_w - T'_0)}|\cos(\Omega)| \quad (4)$$

$$\frac{\partial}{\partial t}(\rho c_p T) + \frac{1}{r}\frac{\partial}{\partial r}\left[\frac{\rho r c_p u T}{A} - \frac{\kappa}{A^2 RePr}\frac{\partial T}{\partial r}\right] + \left[\frac{1}{r}\frac{\partial}{\partial \theta}\frac{\rho c_p v T}{A} - \frac{\kappa}{rA^2 RePr}\frac{\partial T}{\partial \theta}\right] + \frac{\partial}{\partial z}\cdot\left[\rho c_p w T - \frac{\kappa}{RePr}\frac{\partial T}{\partial z}\right] = T\left[\frac{\partial}{\partial t}(\rho c_p) + \frac{1}{A}\frac{\partial}{\partial r}\cdot(\rho c_p u) + \frac{1}{Ar}\frac{\partial}{\partial \theta}(\rho c_p v) + \frac{\partial}{\partial z}(\rho c_p w) + \frac{\rho c_p u}{Ar}\right] \quad (5)$$

The viscous source terms, S_r, S_θ and S_z, appearing in the momentum equations are detailed in the Appendix. The constant-property version of the equations can be obtained by applying the Boussinesq approximation to the gravitational terms and setting the physical properties to their constant reference values in the above equations. In that case, the last terms in Eqs. (2–4) become $(Gr/Re^2)T\cos(\theta)\sin(\Omega)$, $(-Gr/Re^2)T\sin(\theta)\sin(\Omega)$, and $(Gr/Re^2)T|\cos(\Omega)|$, respectively. Note that temperature is chosen, for convenience, as the dependent variable for the energy equation because of the variable-property effects. The consideration of extending this study to two-phase flows in the future also contributed to this decision.

For the variable-property cases, the density of the fluid follows the ideal gas law, and the viscosity and other thermal properties are tabulated values taken from Kays and Crawford.[9] The orientation of the gravity vector with respect to the negative z direction is prescribed by the angle Ω

$$\Omega = \pi - (4\pi/3P) \times MIN\left[t' - (n-1)P, \left(n - \frac{1}{2}\right)P - t'\right]$$

$$(n-1)P \le t' \le \left(n - \frac{1}{2}\right)P$$

$$\Omega = \pi + (4\pi/3P) \times MIN\left[t' - \left(n - \frac{1}{2}\right)P, nP - t'\right]$$

$$\left(n - \frac{1}{2}\right)P \le t' \le nP \qquad (6)$$

where $MIN[A,B]$ represents the minimum of the two quantities A and B. The integer constant n denotes the number of cycles of the jittering motion that have been completed. Ω equals zero when the gravity vector is pointing in the positive z direction and increases counterclockwise. Four main cases and several subcases are examined in this study and can be categorized as follows:

A. A constant-property case without g-jitter. The problem is solved by setting $\Omega = \pi$.

B. A constant-property case with g-jitter. The period of the gravity modulation is 3 s.

C. A variable-property case without g-jitter.

D. A variable-property case with g-jitter. This case is divided further into several subcases:

1) The period of g-jitter cycle is 3 s (base case).

2) At the end of the first cycle in case 1, the gravity vector is held in the negative z direction and the simulation carries on for 3 more s.

3) At the end of the first cycle in case 1, the total gravity level is suddenly dropped from $1g$ to $10^{-2}g$ and the simulation continues for an additional cycle.

4) At the end of the first cycle in case 1, the radial gravity component is set to zero and the simulation carries on for an additional cycle.

5) The same as in case 4, except that the axial gravity component is set to zero, rather than the radial one.

6) The same as in case 4, except that the circumferential gravity component is set to zero, rather than the radial one.

7) The same as in case 1, but the kinematic viscosity of the fluid is artificially increased fourfold.

8) The period of g-jitter cycle is 1 s.

9) The period of g-jitter cycle is 9 s.

Computation

Results presented in the following section are obtained with $Gr = 1.0 \times 10^8$ for the constant-property cases and 1.847×10^7 to 1.847×10^5 for the variable-property cases. The difference in the Grashof numbers arises because different reference property values and/or gravity levels are used in this study. This range of the Grashof number is chosen, as was discussed by Aggarwal et al.,[5] since we are only interested in the multicellular regime. Moreover, all Grashof numbers give a single heater temperature, $T'_w = 1524$ K, so that meaningful comparisons can be made between different cases. For each simulation, a Grashof number is specified first and the reference velocity is obtained by equating to unity the ratio of Grashof number to the Reynolds number squared. The reference pressure is then calculated by setting the Euler number to unity. The side wall and the top wall of the enclosure are adiabatic except for the circular region from $r = 0$ to $r = 0.2$ at the top where the temperature is fixed at T'_w. The bottom wall is kept isothermal at $T'_0 = 300$ K. The no-slip condition applies on all walls for the three velocity components.

The prescribed jittering motion stated in Eq. (6) implies the existence of a plane of symmetry and only the domain between $\theta = 0$ and $\theta = \pi$ needs to be considered. Preliminary simulations which considered the entire circumferential dimension in the base case gave the same solution as that of considering only half of the circumferential domain. Note also that the three-dimensional solution algorithm is employed in

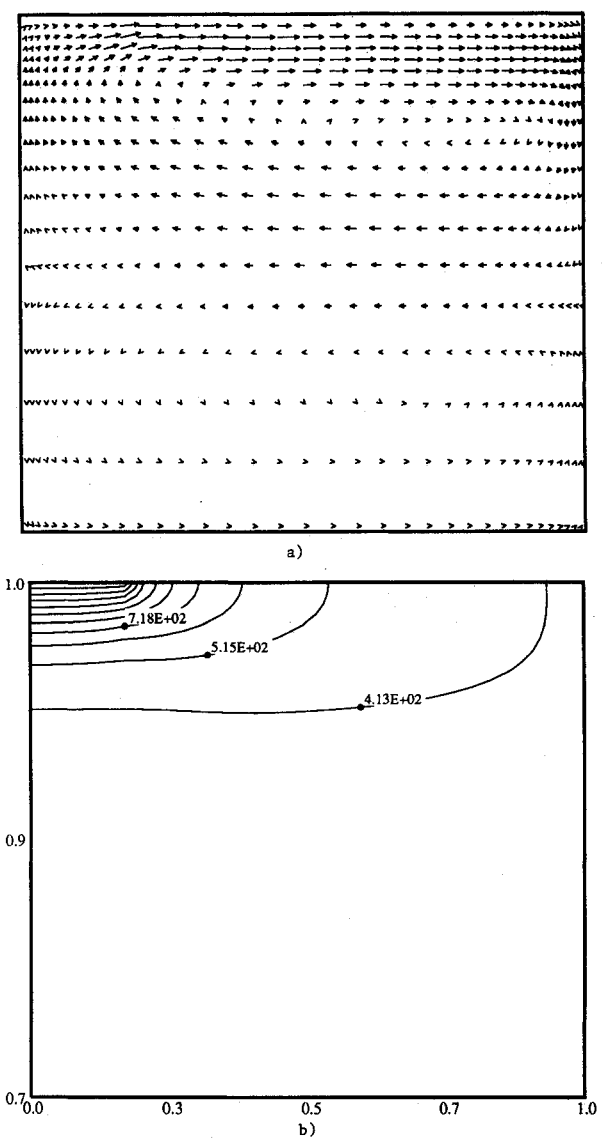

Fig. 2 Velocity vector and temperature contour plots for the constant-property case without g-jitter (maximum vector = 6.36 cm/s; maximum and minimum temperatures are 1430 K and 311 K; time = 6 s.

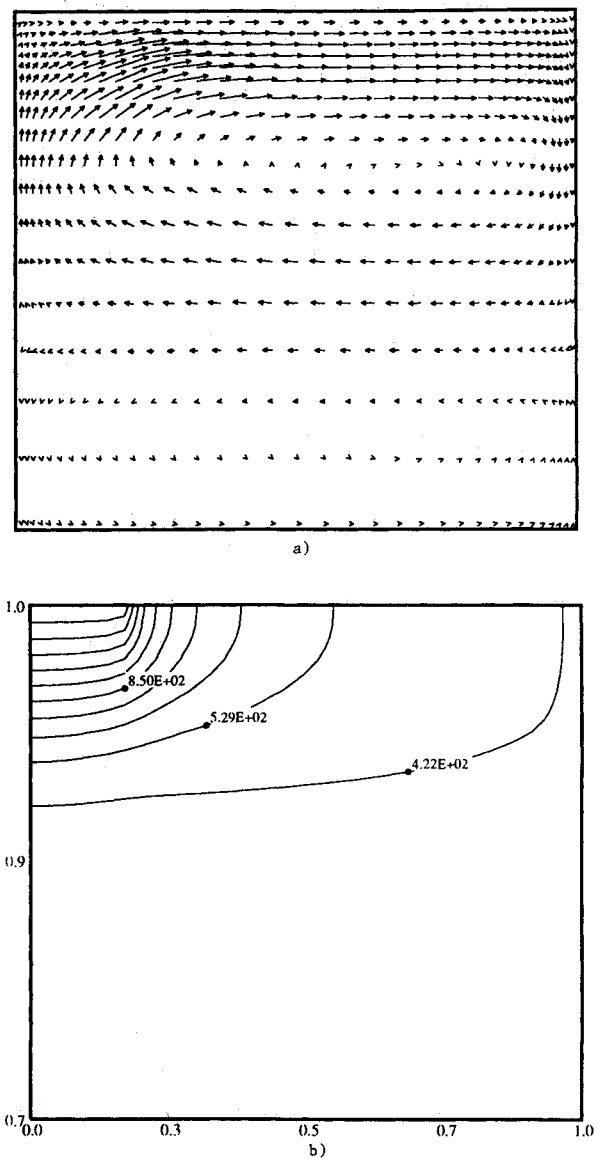

Fig. 3 Velocity vector and temperature contour plots for the variable-property case without g-jitter (maximum vector = 7.828 cm/s; maximum and minimum temperatures are 1490 K and 315 K; time = 6 s.

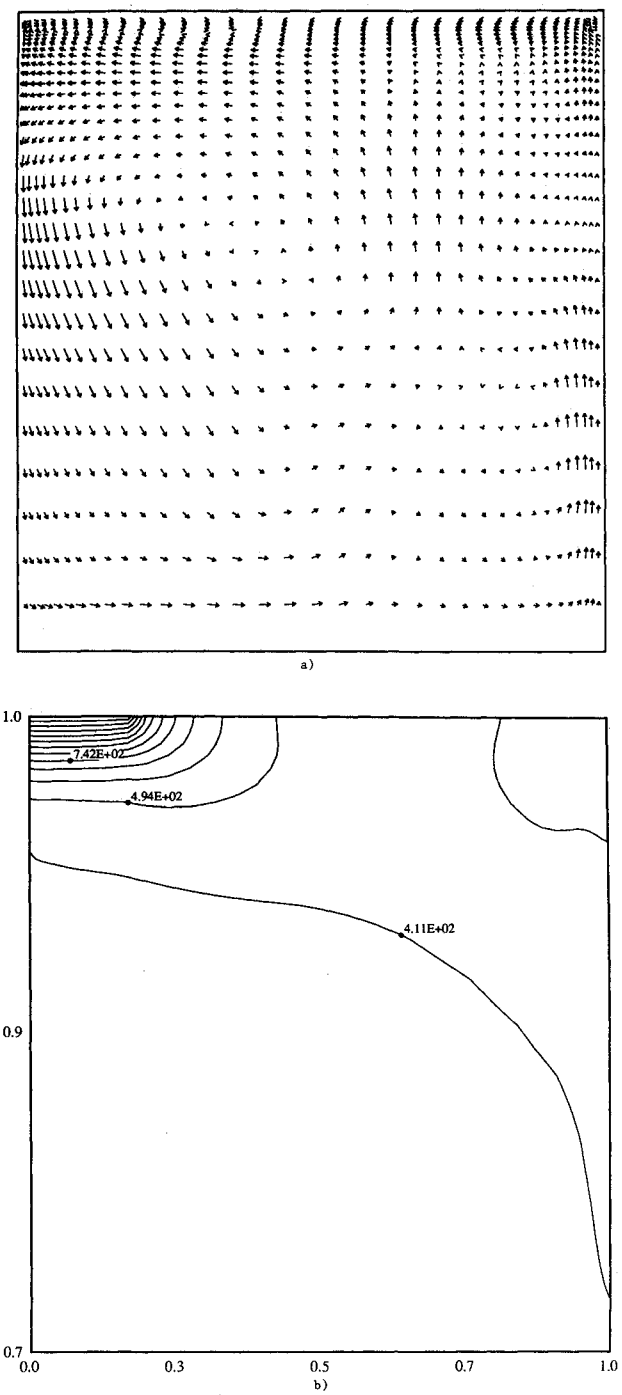

Fig. 4 Velocity vector and temperature contour plots for the constant-property case with g-jitter (maximum vector = 17.76 cm/s; maximum and minimum temperatures are 1400 K and 328 K; time = 6 s, $\theta = 2\pi/3$.

the study even when the flow is expected to be just two-dimensional as a check on the accuracy of the algorithm. The density is normalized by the initial density while other thermal properties are normalized by their individual values at 500 K for the constant-property cases; thermal properties for the variable-property cases are normalized by their values at T'_w. The numerical solution of the equations of motion follows the SIMPLE[10] procedure and uses a hybrid differencing scheme to discretize the governing differential equations. A staggered grid with variable spacings in the radial and axial directions is used in the calculation. All simulations are performed with a 37 × 21 × 33 ($r \times \theta \times z$) mesh except for the cases without gravity modulations, where a 37 × 13 × 33 grid is used. A time step of 1 ms is used for all simulations, although a larger time step could have been used for the simulations without g-jitter. A decrease by one-half of this time step results in negligible changes in the velocity and temperature fields. A 53 × 39 × 49 mesh results in a 5% change in the overall heat transfer rate and the maximum temperature difference (~10%) occurs in the thin region around $z = 0.9$, where the bulk of the heated fluid meets the unheated counterpart, for one cycle of the base case simulation.

Results and Discussion

Velocity and temperature fields within two-dimensional cross sections of the enclosure are presented here. There are two types of cross sections used in the discussion. One is an r-z (vertical) plane and the other is an r-θ (horizontal) plane (Fig. 1). The r-z plane is a rectangular plane, while the r-θ plane is a half-circular plane. The numerical results are shown sometimes in full and sometimes only for the top portion of the vertical plane, but they are always displayed in full from $\theta = 0$ to $\theta = \pi$ in the horizontal plane. Cases without g-jitter are presented first, followed by g-jitter cases of 3-, 1-, and 9-s periods. The g-jitter cases are sometimes referred to alternatively as three-dimensional cases in the discussion.

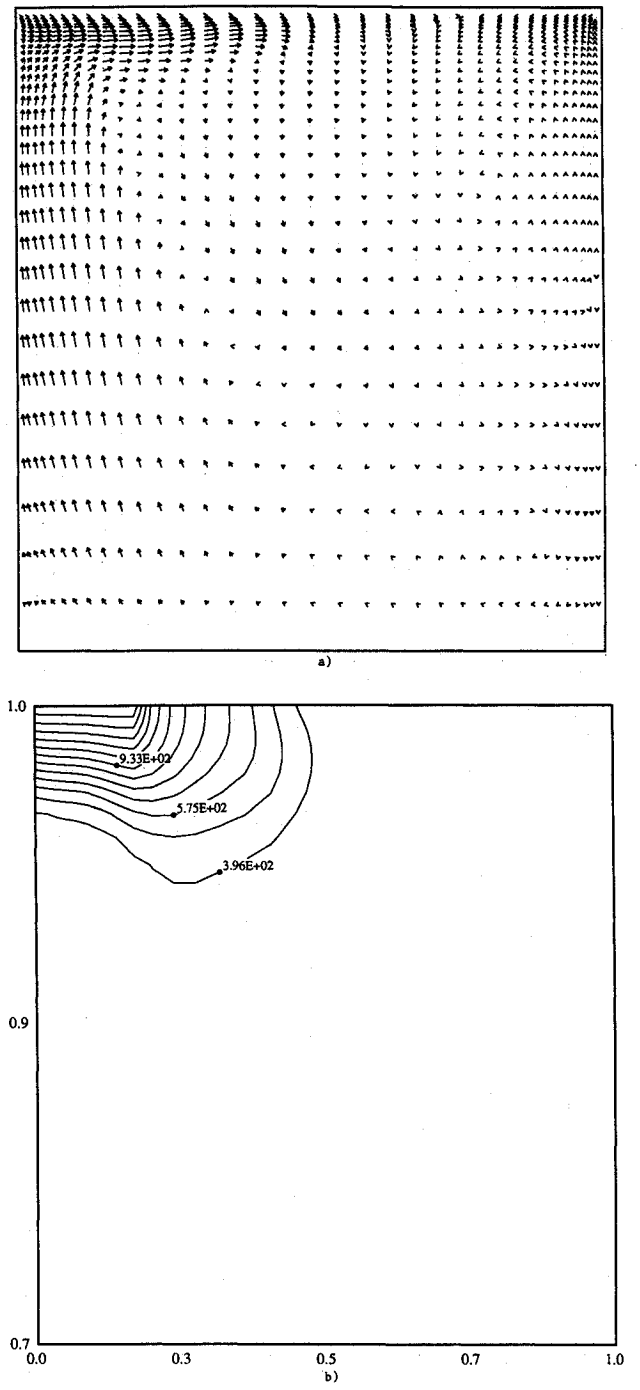

Fig. 5 Velocity vector and temperature contour plots for the variable-property case with g-jitter (maximum vector = 26.885 cm/s; maximum and minimum temperatures are 1470 K and 306 K; time = 6 s, $\theta = \pi/3$.

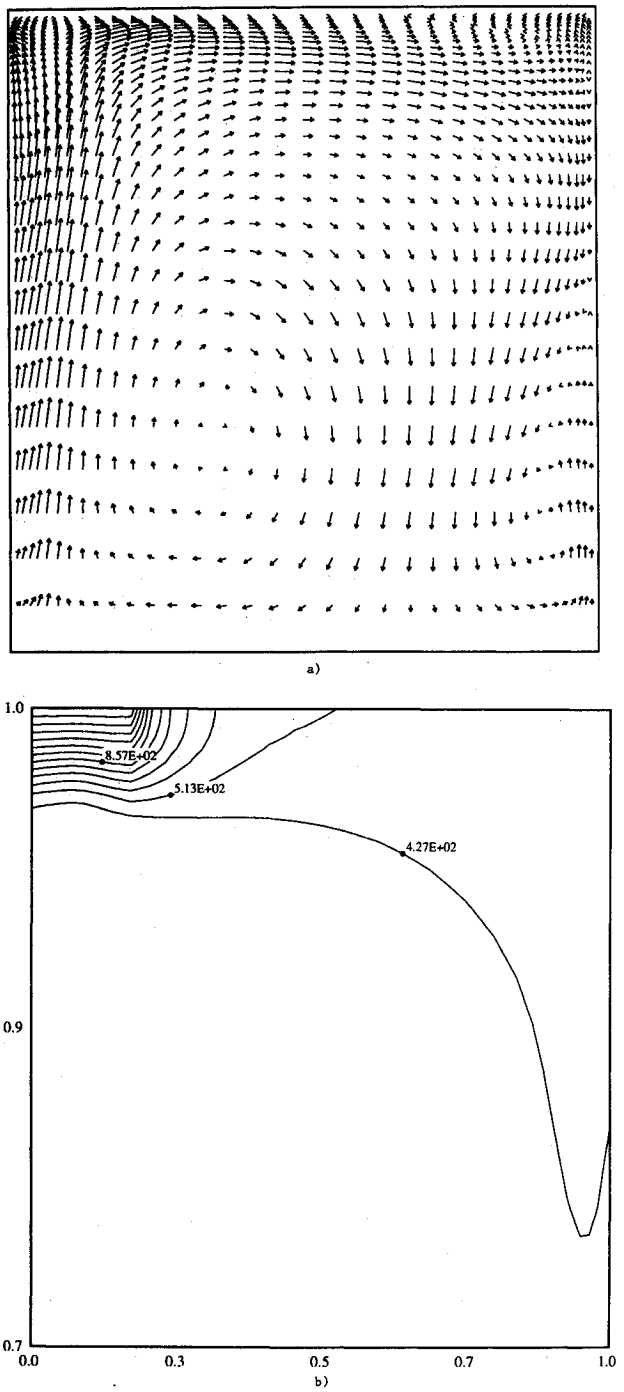

Fig. 6 Velocity vector and temperature contour plots for the variable-property case with g-jitter (maximum vector = 28.081 cm/s; maximum and minimum temperatures are 1460 K and 341 K; time = 6 s; $\theta = 2\pi/3$.

Figures 2a and 2b show the velocity and the temperature fields in a vertical plane for the constant-property case without gravity modulations at $t' = 6$ s. Only less than a third of the vertical plane is shown here for clarity. The computation shows that, as expected, the flow and thermal fields are identical in all vertical planes of the computational domain. An established recirculation cell and a developing, counter-rotating cell are present in the flow. The temperature contours, stretching in the radial direction, indicate that the thermal energy transport in the flow is primarily by convection. The secondary cell is induced mainly by viscosity. The magnitude of the velocity diminishes quickly going from the main circulation cell to the still developing, secondary cell. Figures 3a and 3b show the temperature and velocity fields for the variable-property case without g-jitter at $t' = 6$ s. The velocity vector plot shows that the flow field has basically the same structure as that of the constant-property case, except for a slightly larger, main circulation cell. The temperature contours also penetrate deeper into the cold fluid for the variable-property case. The secondary cell has established itself completely in Fig. 3a but is not shown entirely in the plot.

Figures 4a and 4b are a full-size vector plot and a zoom-in temperature contour plot in the $\theta = 2\pi/3$ vertical plane for the three-dimensional, constant-property case at $t' = 6$ s. Both plots present drastically different pictures of flow structure and temperature field from those without g-jitter. One can identify three circulation cells lined up diagonally from the top left corner to the bottom right corner and the strong fluid motion in the circumferential direction. The maximum velocity in this plane is much larger than that of Fig. 2a, and

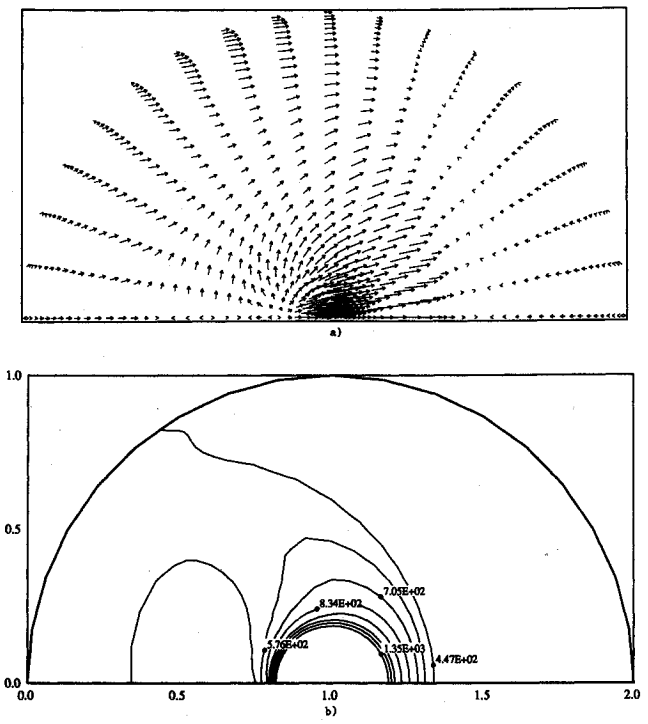

Fig. 7 Velocity vector and temperature contour plots for the variable-property case with g-jitter (maximum vector = 5.28 cm/s; maximum and minimum temperatures are 1480 K and 317 K; time = 6 s, z = 0.997.

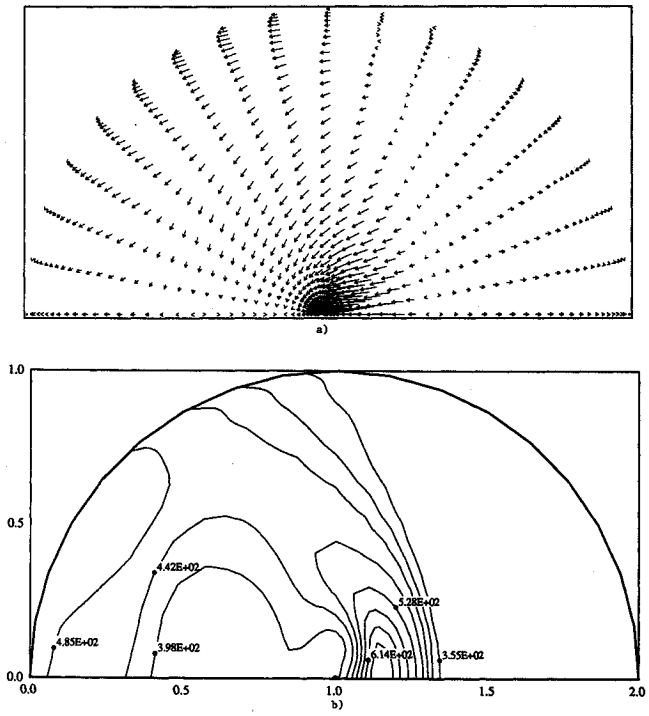

Fig. 8 Velocity vector and temperature contour plots for the variable-property case with g-jitter (maximum vector = 29.65 cm/s; maximum and minimum temperatures are 700 K and 312 K; time = 6 s, z = 0.949.

an isolated packet of fluid is found at the top right corner in the temperature contour plot in Fig. 4b. Figures 5a and 5b show a full-scale velocity vector plot and a zoom-in temperature contours plot in the $\theta = \pi/3$ vertical plane at $t' = 6$ s for the three-dimensional, variable-property case. They also show significant changes in the flow structure and temperature field and strong three-dimensional effects compared to Fig.

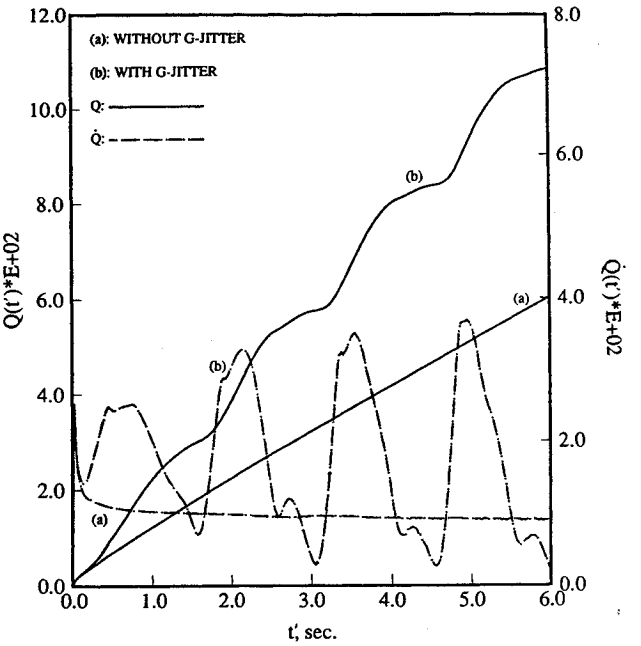

Fig. 9 Thermal histories of the constant-property cases.

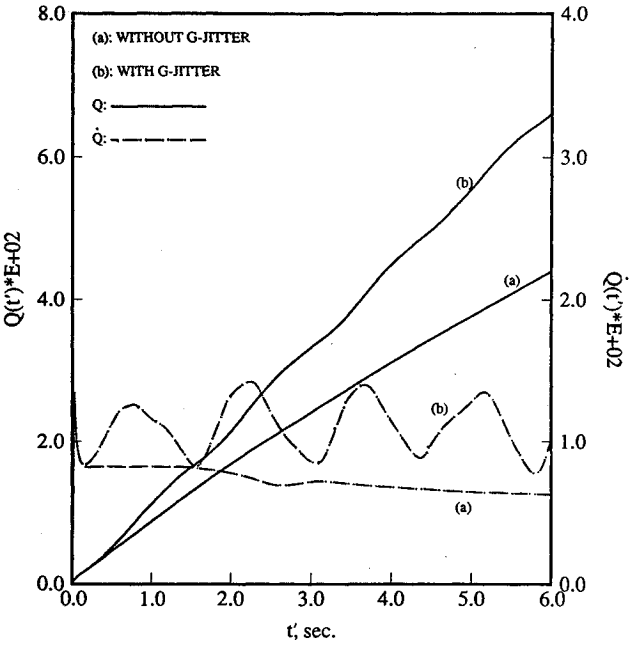

Fig. 10 Thermal histories of the variable-property cases.

3. The conduction-like temperature field is a result of strong convective flow (*opposite* to the heat transfer direction when there is no g-jitter) toward the quarter between $\theta = \pi/2$ and $\theta = \pi$ due to the imposed gravitational field. Flow adjustment to the coming reversal of the radial and circumferential gravity components is also seen at the top of the velocity vector plot. Figures 6a and 6b show the velocity and temperature fields in the $\theta = 2\pi/3$ vertical plane for the same case. Three-dimensional effects and more complicated flow patterns are visible in this plane because of stronger interaction between the hot and cold fluids at this instant. A large, skewed circulating cell and a smaller one close to the bottom portion of the right boundary can be identified from the vector plot. The downward draft from the larger circulation cell is responsible for transporting hot fluid into lower axial positions, as is seen in Fig. 6b.

Figures 7a and 7b show the velocity vector and temperature contours plots in a horizontal plane at $z = 0.997$ and $t' =$

6 s. The vector plot shows that the hotter (lighter) fluid between $\theta = \pi/2$ and $\theta = \pi$ responds to the change of gravity much faster than the colder (heavier) fluid between $\theta = 0$ and $\theta = \pi/2$ does. The signature from the heat source can also be seen in Fig. 7b to the right of an isolated fluid packet which is created by the upwelling of fluid from lower z positions (see Fig. 6a). The unequal spacings between the nearly-concentric temperature contours indicate that the convective transport is stronger than the conduction. Figures 8a and 8b show the velocity and temperature fields at a lower position, $z = 0.949$. The change in direction of the velocity vectors between Figs. 7a and 8a indicates a circulation in the flow. The maximum magnitude of velocity has increased from 5.28 to 29.65 cm/s due to reduced wall effects. The temperature of the hot fluid at this height is much lower than those at the previous location. However, the interaction between the heated and cold fluid is stronger at this axial position due to proximity. The colder fluid, with higher density and inertia, can better resist reversing its direction of motion dictated by the new directions of the radial and circumferential gravity components. The signature from the heat source is completely smeared by the strong, natural convective transport and larger, isolated fluid packets also exist at this axial location.

To better understand the overall effects of g-jitter in heat transfer for the entire system, a quantity Q is defined, for convenience, as follows:

$$Q = \sum (\rho c_p T V)$$

where the summation is performed over the entire enclosure. This quantity is easy to calculate and equal to the nondimensional system enthalpy for the constant-property cases. For the variable-property cases, it is greater than but directly proportional to the nondimensional system enthalpy. Figure 9 compares the transient evolutions of Q and its rate of increase for the constant-property cases with and without g-jitter effects. While Q increases linearly during most of the time in the case without g-jitter, the three-dimensional case exhibits a periodic increase of Q. The leveling-off periods on the Q curve with g-jitter effects always occur before a reversal in direction of the radial and circumferential gravity components. The rate of increase of Q is, for practical purposes, constant for the no g-jitter case after 2.5 s which also corresponds to the complete establishment of the main recirculating cell in the flowfield. The rate of increase for the three-dimensional case, on the other hand, oscillates strongly about an increasing mean value. Figure 10 shows the thermal histories for the variable-property cases with and without g-jitter effects. Variable properties of the working fluid (air in this case) dampen the leveling-off periods in Fig. 9, but the prescribed gravity modulation still gives rise to a periodic increase of heat transfer. An inflection point exists at $t \simeq 2.9$ s in the otherwise smooth rate curve for the no g-jitter case. This time corresponds roughly to the time required for the fluid to complete one circulation in the main recirculation cell.

Figures 11a and 11b display variations of Q and $\dot{Q}$ to compare the effect of the radial, circumferential and axial gravity

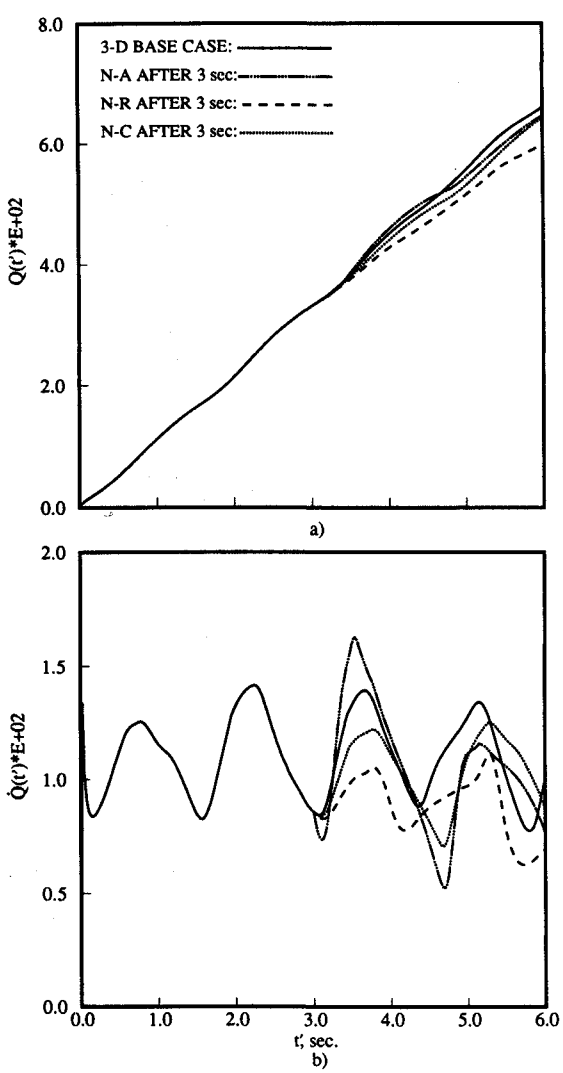

Fig. 11 Effects of various gravity components on heat transfer.

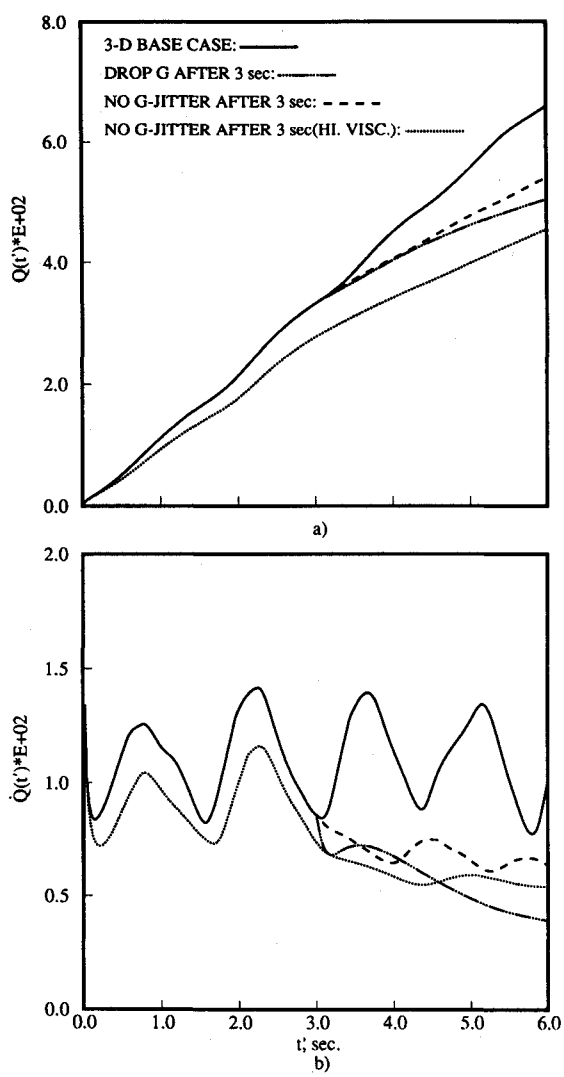

Fig. 12 Effects of gravity, g-jitter, and viscosity on heat transfer.

components of the prescribed gravitational field. N-A stands for the no axial gravity case, N-R for the no radial gravity case, and N-C for the no circumferential gravity case, respectively. The quantity Q of the N-R system and the N-C system is always lower than that of the base case after $t' = 3$ s. This indicates that the radial and the circumferential gravity components enhance the heat transfer to the fluid. This is consistent with two-dimensional results from Kamotani et al.[8] Moreover, the radial component is more effective than the circumferential one. The same observations can also be drawn from the rate histories of the three cases. The curve for the base case envelopes the curves for the N-R and N-C cases and, at the same time, the curve for the N-C case envelopes the one for the N-R case. The axial component has a different and ambiguous nature. It seems to inhibit the heat transfer more than to enhance it, at least on a short time basis. Therefore, eliminating the axial gravity component has the same effect as increasing the radial or circumferential gravity component. This can explain the higher heat transfer rate for the N-A system immediately after $t' = 3$ s. However, Q and its rate for the N-A system drop below that of the base case after about 1.6 s. The radial and circumferential components help move hot fluid away from and bring colder fluid toward the heat source, but they seem unable to do this effectively unless there is a reduction of the axial component. The long-term thermal behavior of the N-A system is not clear at this stage.

Figures 12a and 12b compare the effects of reduced gravity, gravity modulation, and viscosity. The results indicate that

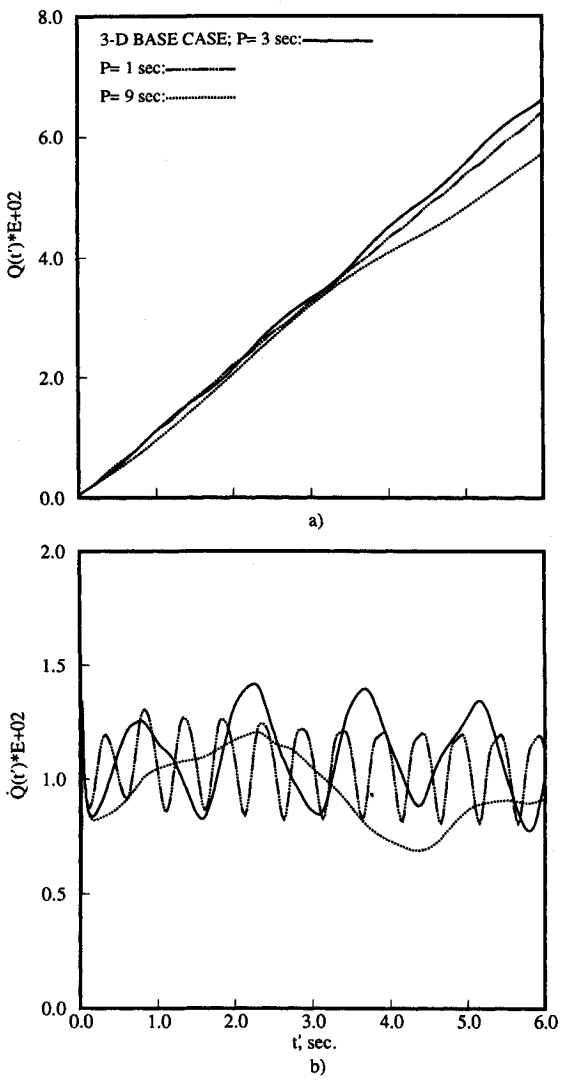

Fig. 13 Effects of the g-jitter frequency on heat transfer.

reducing the total gravity level is more efficient than eliminating g-jitter entirely in reducing the effects of gravity modulations after a system has been disturbed. This has two important consequences. It implies, first, that a microgravity environment can effectively reduce the effects of gravity and its modulations for acceleration-sensitive experiments. Second, once an experiment has been affected by external accelerations, eliminating the unwanted accelerations and relying on fluid viscosity to dampen the effects of g-jitter may not be effective. However, the viscosity of the working fluid plays an important role in controlling the overall heat transfer. It also determines the postjittering behavior of the fluid inside the enclosure, as demonstrated by the case with the normal viscosity and the case with four times the normal viscosity. Figures 13a and 13b show the thermal histories of three different cases, corresponding to 3-, 1-, and 9-s g-jitter periods, respectively. There exists a coupling between the flow structure and the overall heat transfer into the system. The period of the base case in the figure is approximately equal to the circulation time of the main recirculation cell in the no g-jitter case. A resonant effect causes the base case to have the highest rate of heat transfer. Away from this characteristic time, the jittering frequency determines the ranks of the other two cases.

Conclusions

A thermally buoyant flow in a cylindrical enclosure with nonuniform heating from above is examined and many observations are made. Both the temperature and velocity fields respond to the imposed gravity modulations. The imposed gravity modulations result in strong three-dimensional effects, and heat transfer from the heat source into the fluid is increased significantly. The additional thermal energy can amount to as much as 47% of the total energy of the two-dimensional system at the end of a 6-s simulation. The temperature contours at various circumferential locations, depending on the time in a g-jitter cycle, may display conduction-like patterns. Isolated hot and cold fluid packets are common in the three-dimensional flows because a finite period of time is needed for the fluid to respond to the imposed, continuous gravity modulations. The variable properties of the working fluid smoothen the transitions at the half of a g-jitter cycle where a change of direction in both the radial and the circumferential gravity components occur. The variable-property temperature field is more complicated than the constant-property one, and larger local maximum velocity is created because variable accelerations now apply to fluids with different densities. The signature from the heat source is clear for a short distance below it, but the signature fades faster for the variable-property cases on the account of stronger convection and nonlinear interaction between the temperature and velocity fields.

To counter the effects of g-jitter, this study finds that reducing the magnitude of gravity is more promising than eliminating the g-jitter sources. This implies that, once a system is contaminated by extra accelerations, the only effective measure to quickly restore the system back to its predisturbed stage is to decrease the total acceleration level. Momentum diffusion by viscosity alone may not be efficient to eliminate the unwanted effects of acceleration in a short period. This is expected to be more so for less viscous fluids, like gases. In addition, a higher viscosity of the working fluid decreases the overall heat transfer due to reduced Reynolds and Nusselt numbers, and the kinematic viscosity determines the postjittering behavior of the fluid. The three components of gravity have different degrees of effectiveness in enhancing the total heat transfer. The radial and circumferential components in this study play more or less the same role as far as overall heat transfer is concerned, but the axial component's role is somewhat obscure. Furthermore, the radial component is more potent than the circumferential one in this respect. Reducing the axial gravity level increases the total heat tranfer, but it is only a short-term effect. The long-term effect of the axial

gravity component requires further studies, but its influence does not seem to be negligible.

Appendix

$$S_r = \frac{1}{r}\frac{\partial}{\partial r}\left(\frac{\mu r}{A^2 Re}\frac{\partial u}{\partial r}\right) + \frac{1}{r}\frac{\partial}{\partial \theta}\left[\frac{\mu r}{A^2 Re}\frac{\partial}{\partial r}\left(\frac{v}{r}\right)\right] + \frac{\partial}{\partial z}\left(\frac{\mu}{ARe}\frac{\partial w}{\partial r}\right) + \frac{\rho v^2}{Ar} - \frac{2\mu}{A^2 r^2 Re}\left(\frac{\partial v}{\partial \theta} + u\right) - \frac{2}{3r}\frac{\partial}{\partial r}\left\{\frac{\mu r}{A^2 Re}\left[\frac{1}{r}\frac{\partial}{\partial r}(ru) + \frac{1}{r}\frac{\partial v}{\partial \theta} + A\frac{\partial w}{\partial z}\right]\right\} + \frac{2\mu}{3rA^2 Re}\left[\frac{1}{r}\frac{\partial}{\partial r}(ru) + \frac{1}{r}\frac{\partial v}{\partial \theta} + A\frac{\partial w}{\partial z}\right]$$

$$S_\theta = \frac{1}{r^2}\frac{\partial}{\partial r}\left(\frac{\mu r}{A^2 Re}\frac{\partial u}{\partial \theta}\right) + \frac{1}{r}\frac{\partial}{\partial \theta}\left(\frac{\mu}{rA^2 Re}\frac{\partial v}{\partial \theta}\right) + \frac{\partial}{\partial z}\left(\frac{\mu}{rARe}\frac{\partial w}{\partial \theta}\right) + \frac{1}{r}\frac{\partial}{\partial \theta}\left(\frac{2\mu}{rA^2 Re}\frac{u}{r}\right) + \frac{\mu}{A^2 Re}\frac{\partial}{\partial R}\left(\frac{v}{r}\right) - \frac{\rho uv}{rA} - \frac{1}{r}\frac{\partial}{\partial r}\left(\frac{\mu v}{A^2 Re}\right) - \frac{2}{3r}\frac{\partial}{\partial \theta}\left\{\frac{\mu}{A^2 Re}\left[\frac{1}{r}\frac{\partial}{\partial r}(ru) + \frac{1}{r}\frac{\partial v}{\partial \theta} + A\frac{\partial w}{\partial z}\right]\right\}$$

$$S_z = \frac{1}{r}\frac{\partial}{\partial r}\left(\frac{\mu r}{ARe}\frac{\partial u}{\partial z}\right) + \frac{1}{r}\frac{\partial}{\partial \theta}\left(\frac{\mu}{ARe}\frac{\partial v}{\partial z}\right) + \frac{\partial}{\partial z}\left(\frac{\mu}{Re}\frac{\partial w}{\partial z}\right) - \frac{2}{3}\frac{\partial}{\partial z}\left\{\frac{\mu}{ARe}\left[\frac{1}{r}\frac{\partial}{\partial r}(ru) + \frac{1}{r}\frac{\partial v}{\partial \theta} + A\frac{\partial w}{\partial z}\right]\right\}$$

Acknowledgments

This work is sponsored by NASA Lewis Research Center under Grant NAG3-627, and H. D. Ross is the Project Monitor. Trial runs for most of the cases were conducted with a Convex C240 supercomputer at the Office of Academic Computing of the University of California at Irvine. Some production runs were carried out by the Cray-2 supercomputer at NASA Ames Research Center. The majority of production runs were conducted with the Cray Y-MP supercomputer at the San Diego Supercomputing Center. Special thanks to Paolo Bellomi and to C. H. Chiang for help on graphics.

References

[1]Sirignano, W. A., "A Critical Discussion of Theories of Flame Spread Across Solid and Liquid Fuels," *Combustion Science and Technology*, Vol. 6, No. 1, 1972, pp. 95–105.

[2]Aziz, K., and Hellums, J. D., "Numerical Solution of the Three-Dimensional Equations of Motion for Laminar Natural Convection," *Physics of Fluids*, Vol. 10, No. 2, 1967, pp. 314–325.

[3]Ozoe, H., Fujii, K., Lior, N., and Churchill, S. W., "Long Rolls Generated by Natural Convection in an Inclined, Rectangular Enclosure," *International Journal of Heat and Mass Transfer*, Vol. 26, No. 10, 1983, pp. 1427–1438.

[4]Yang, H. Q., Yang, K. T., and Lloyd, J. R., "Flow Transition in Laminar Buoyant Flow in a Three-Dimensional Tilted Rectangular Enclosure," *Proceedings of the Seventh Heat Transfer Conference*, 1986, pp. 1495–1500.

[5]Aggarwal, S. K., Iyengar, J., and Sirignano, W. A., "Enclosed Gas and Liquid with Nonuniform Heating from Above," *International Journal of Heat and Mass Transfer*, Vol. 29, No. 10, 1986, pp. 1593–1604.

[6]Ross, H. D., Schiller, D. N., Disimile, P., and Sirignano, W. A., "Behavior in Normal and Reduced Gravity of an Enclosed Liquid/Gas System with Nonuniform Heating from Above," AIAA Paper 89–0070, Jan. 1989 (see also NASA Technical Memorandum 101471).

[7]Gresho, P. M., and Sani, R. L., "The Effects of Gravity Modulation on the Stability of a Heated Fluid Layer," *Journal of Fluid Mechanics*, Vol. 40, Pt. 4, 1970, pp. 783–806.

[8]Kamotani, Y., Prasad, A., and Ostrach, S., "Thermal Convection in an Enclosure Due to Vibrations Aboard Spacecraft," *AIAA Journal*, Vol. 19, No. 4, 1981, pp. 511–516.

[9]Kays, W. M., and Crawford, M. E., *Convective Heat and Mass Transfer*, 2nd ed., McGraw-Hill, New York, 1980, p. 388.

[10]Patankar, S. V., *Numerical Heat Transfer and Fluid Flow*, McGraw-Hill, New York, 1981, pp. 123–131.